arXiv:2101.08646v1 [physics.comp-ph] 20 Jan 2021

New developments regarding the JOREK solver and physics based preconditioner

I Holod [1,2], M Hoelzl [2], P S Verma[2], GTA Huijsmans[3,4], R Nies [5,6], and JOREK Team[7]

[1]Max Planck Computing and Data Facility (MPCDF)
[2]Max Planck Institute for Plasma Physics, Boltzmannstr. 2, 85748 Garching b. M., Germany
[3]CEA, IRFM, 13108 Saint-Paul-Lez-Durance, France
[4]Eindhoven University of Technology, P.O. Box 513, 5600 MB Eindhoven, The Netherlands
[5]Department of Astrophysical Sciences, Princeton University, Princeton, NJ, 08543, USA
[6]Princeton Plasma Physics Laboratory, Princeton, NJ, 08540, USA
[7]Refer to the author list of [M Hoelzl, G T A Huijsmans, S J P Pamela, M Becoulet, E Nardon, F J Artola, B Nkonga et al, Nuclear Fusion (submitted)]

Contents

1 Introduction **2**
1.1 JOREK . . . 2
1.2 Sparse Matrix Solvers . . . 5
1.3 Phases in a time step . . . 6
1.4 Setup for the numerical tests . . . 7
1.5 Outline . . . 8

2 Developments performed in this work **8**
2.1 Construction of preconditioning matrices . . . 8
2.2 New solver interfaces . . . 8
2.3 Generalization of the preconditioner for mode groups . . . 10

3 Benchmarks for the developments performed **12**
3.1 Preconditioner matrix assembly . . . 12
3.2 Comparison of PaStiX and STRUMPACK solver performance . . . 12
3.3 Comparison between real and complex solvers in the preconditioner . . . 17
3.4 Assessment of computational efficiency with mode groups in the preconditioner . 19

4 Summary **23**

Abstract

The JOREK extended magneto-hydrodynamic (MHD) code is a widely used simulation code for studying the non-linear dynamics of large-scale instabilities in divertor tokamak plasmas. Due to the large scale-separation intrinsic to these phenomena both in space

and time, the computational costs for simulations in realistic geometry and with realistic parameters can be very high, motivating the investment of considerable effort for optimization. The code is usually run with a fully implicit time integration allowing to use large time steps independent of a CFL criterion. This is particularly important due to the fast time scales associated with MHD waves and fast parallel heat transport. For solving the resulting large sparse-matrix system iteratively in each time step, a physics-based preconditioner building on the assumption of a weak coupling between the toroidal harmonics is applied. The solution for each harmonic matrix is determined independently in this preconditioner using a direct sparse matrix library. In this article, a set of developments regarding the JOREK solver and preconditioner is described, which lead to overall significant benefits for large production simulations. This comprises in particular enhanced convergence in highly non-linear scenarios and a general reduction of memory consumption and computational costs. The developments include faster construction of preconditioner matrices, a domain decomposition of preconditioning matrices for solver libraries that can handle distributed matrices, interfaces for additional solver libraries, an option to use matrix compression methods, and the implementation of a complex solver interface for the preconditioner. The most significant development presented consists in a generalization of the physics based preconditioner to "mode groups", which allows to account for the dominant interactions between toroidal Fourier modes in highly non-linear simulations. At the cost of a moderate increase of memory consumption, the technique can strongly enhance convergence in suitable cases allowing to use significantly larger time steps. For all developments, benchmarks based on typical simulation cases demonstrate the resulting improvements.

1 Introduction

Non-linear extended MHD allows to describe a huge variety of different large-scale instabilities in magnetically confined fusion plasmas accurately and with lower computational costs than (gyro)kinetic approaches. Numerically, however, there are significant challenges to overcome: large spatial and temporal scale separations need to be bridged. Highly anisotropic heat transport, fast plasma flows and a large scale separation in time render it virtually impossible to simulate realistic parameters without an implicit time integrator.

The following Sections 1.1 to 1.4 provide background on the JOREK code and the sparse matrix solvers, explain the numerical stages executed during a time step, and describe the setup used for the numerical tests. Section 1.5 contains the outline of the main part of the article, which describes the developments implemented before they are tested via a series of benchmarks.

1.1 JOREK

JOREK [1, 2] is a state-of-the-art code for the simulation of large-scale instabilities in tokamaks (magnetic confinement fusion devices). It solves extended reduced [3] or full [4] MHD equations using a 2D iso-parametric G^1 continuous finite element discretization

combined with a toroidal Fourier decomposition [5]. Main applications are simulations addressing the dynamics of major disruptions including vertical displacement events and runaway electrons as well as edge localized modes. The goal is to advance the physics understanding for these potentially very harmful phenomena and to develop reliable control schemes applicable in present and future fusion devices.

A free boundary and resistive wall extension exists [6] and a framework for kinetic effects is available [7]. The time integration is fully implicit such that a very large – and, due to the properties of the equations, badly conditioned – sparse matrix system needs to be solved in every time step. The present article describes improvements of the computational efficiency of the code by a variety of different approaches enhancing the solver performance. We describe the key properties of the JOREK solver and the sparse matrix system in the following Subsections 1.1.1 and 1.1.2.

1.1.1 Solver

Due to the fully implicit time integration used in JOREK, a large sparse matrix system connecting all degrees of freedom needs to be solved in every time step (see Section 1.1.2 for details). Two main options are available for that: when the problem size is small, in particular for axisymmetric cases, a direct sparse matrix solver is applied to the complete system (see Section 1.2 for details on direct sparse matrix solvers). Second option is applied for the large problem sizes typically encountered in real-life applications: the system is solved iteratively with a restarted GMRES algorithm. Since the system is badly conditioned, a physics-based preconditioner needs to be applied: The matrix P containing only the diagonal blocks of the matrix corresponding to the toroidal Fourier modes is used for left preconditioning, while all off-diagonal blocks are neglected. A schematic representation for a small case with the toroidal modes $n = (0, 1, 2, 3)$ is shown in Figure 1. For the preconditioner, linear systems $P\,y = c$ need to be solved in each GMRES iteration as well as for the initial guess. Due to the block diagonal structure of P, the system can be solved independently and in parallel for each toroidal mode with (direct) sparse matrix libraries, which greatly reduces the overall memory consumption and computational costs compared to directly solving the complete system. The preconditioning matrix P can usually be reused for many time steps thus saving on the expensive LU-factorization. In the linear phase of the physical system's evolution, when the mode amplitudes are small and mode coupling is negligible, the preconditioner matrix P is an almost exact approximation of the full matrix A such that the iterative solver usually converges in a single iteration. However, when the problem becomes non-linear such that the coupling between toroidal modes cannot be neglected any more, the preconditioner becomes far less efficient, and consequently the GMRES convergence deteriorates. This poor approximation of A by the preconditioning matrix P is one of the main challenges for the efficiency of the JOREK solver. Besides that, the large memory consumption of the LU decomposed preconditioner matrix blocks and the limited parallel scalability of the direct sparse matrix solvers are additional challenges to be faced. Also the construction of the preconditioner matrix blocks – presently done by extracting them from the global matrix via expensive MPI communication – constitutes a computational

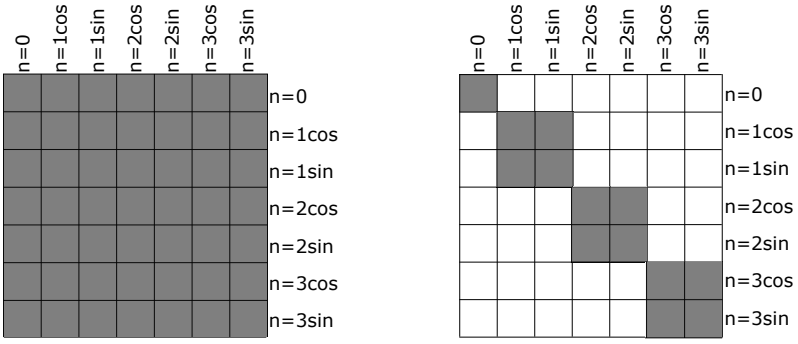

Figure 1: The matrix structure is shown for a simple example case with the toroidal modes $n = (0, 1, 2, 3)$. The **left figure** shows the structure of the complete matrix A, where axisymmetric $n = 0$ has half as many degrees of freedom as the other modes. The **right figure** shows the preconditioning matrix P like it is normally used in JOREK. Only the diagonal parts are retained such that each mode is assumed decoupled from the others in the preconditioner and the sparse diagonal blocks can be solved independently from each other.

bottleneck.

In the present work, we address these challenges, leading to a significant step forward in code efficiency: the construction of the preconditioner matrices is performed directly, avoiding communication overhead (Section 2.1), new solver interfaces are built to exploit advanced features, including complex representation of sparse matrices (Section 2.2). Finally, a generalization of the preconditioner is developed, which allows to approximate the matrix A more accurately in highly non-linear scenarios (Section 2.3). The performance of the new developments is evaluated in Section 3.

1.1.2 Matrix properties

Here we describe the sparse matrix properties for a typical large problem size of 30 thousand grid nodes, 8 physical variables, 4 degrees of freedom per grid node, and 41 toroidal harmonics – this is counting cosine and sine components separately such that this corresponds to toroidal modes $n = (0 \ldots 20)$.

Global matrix The total dimension of the matrix corresponding to this problem size is about 40 million. All node variables are typically coupled with each other, and, additionally, with eight neighboring grid nodes[1]. This leads to about 12 thousand non-zero entries in each matrix row and about 500 billion non-zero entries in the whole matrix, which requires about 4 TB of main memory for storing the double precision floating point numbers. Additional memory is needed for storing the matrix indices, depending on the sparse matrix format used. For the coordinate format using 2 integer

[1] At special points like the grid axis and the X-point, this may be different. Depending on the boundary conditions, the connectivity can also be different there.

indices of 4-byte each, the total memory requirement for the matrix storage is about 8 TB. In case of compressed sparse row (CSR) format, the amount of memory needed to store the location of the entries is reduced by nearly 50%, so totally a bit more than 6 TB would be required. In JOREK, the matrix is constructed in coordinate format and the preconditioner matrices are stored in CSR format.

As shown above, due to the locality of the 2D Bezier basis functions, the global matrix is sparse with only one out of 3000 matrix entries different from zero in each row or, respectively, column. Since the matrix in our example does not fit into the memory of one typical compute node (100-200 GB), we use domain decomposition to construct matrix in a distributed way. If in this case we use 84 compute nodes with 4 MPI tasks per node (336 MPI tasks in total), each MPI task is responsible for constructing the matrix contributions by about 90 grid elements. This way, roughly 25 GB of storage are needed per MPI task for the distributed global matrix, i.e., about 100 GB per compute node. The matrix construction on each MPI task is OpenMP parallelized. If we assume 8 OpenMP threads per MPI task, each thread is responsible for creating the matrix contributions of about 10 grid elements (called elementary matrices). The elementary matrices are dense and have a dimension of about 5000 (4 nodes times 4 degrees of freedom times 8 variables times 41 Fourier harmonics) requiring about 200 MB of main memory each. The matrix is constructed using fast Fourier transform. When a single toroidal Fourier mode is used (in test simulation), direct integration is applied instead.

Preconditioner matrix For the considered example, each block of the preconditioner matrix P has a dimension of about 2 million, and about 600 non-zero entries per matrix row, such that each of the block-matrices has about 1 billion non-zero entries consuming about 12 GB of main memory in CSR format. Each of these blocks corresponds to a particular toroidal mode n, and need to be LU decomposed in the preconditioning, see Section 1.1.1. All blocks together require about 250 GB of memory. The block-matrix corresponding to $n = 0$ is smaller by a factor of two in dimension and by a factor of four in the number of non-zero entries (since $n = 0$ has only axisymmetric component). During LU-factorization (see Section 1.1.1), the memory consumption increases significantly due to the fill-in.

1.2 Sparse Matrix Solvers

A linear system of equations $B\,x = b$ is solved in JOREK using a solver library, where matrix B corresponds either to the full system A for small cases or to the diagonal block P_i of the preconditioning matrix P.

The matrix B is sparse as shown in the previous section. Despite its large size due to the numerous degrees of freedom, it consists mostly of zero entries, since interactions are localized in space by the local basis functions. Naively using full matrix factorisation algorithms on a sparse system would prohibitively increase the number of operations and the required memory, and therefore special techniques must be employed. We remind briefly here of the main aspects of sparse matrix solving and matrix compression

techniques, which can further reduce the computational cost and memory requirements. Readers interested in a more detailed treatment are referred to [8] and references therein.

One of the main problems occurring during LU factorization of a sparse matrix is fill-in, i.e., the number of entries in the LU factors can greatly exceed that of the original matrix B. During the *analysis* phase, it is therefore attempted to determine the optimal order in which the entries in L and U matrices should be computed such as to minimise fill-in. The sparse matrix is represented as a graph where each vertex represents an interaction, i.e., a connection between nodes i and j is equivalent to $B_{i,j} \neq 0$. The factorisation is then reflected by an elimination tree traversing this graph. Standard tools to determine the ordering include METIS [9] and SCOTCH [10], which use nested dissection algorithms, where the graph is recursively partitioned until the size is sufficiently reduced to allow for local ordering methods. During the *factorisation* phase, the elimination tree is traversed, starting from the tree leafs up to its root. Upon elimination of a node, all of its parents up the tree must be updated, which can be performed either immediately (right-looking), only when the parent node is factorised (left-looking) or in a combination of the two where contributions from multiple nodes are grouped together (multifrontal). The sparse matrix solvers used in JOREK are right-looking PaStiX [11, 12] or multifrontal MUMPS [13, 14] and STRUMPACK [15] (the interface for the latter was developed as part of this work). Finally, during the *solution* phase, the vector x is obtained by solving the systems $L\,y = b$ and $U\,x = y$ through back and forward-substitution.

Matrix compression techniques often offer further reductions in memory requirements and/or computational cost for sparse matrix systems. In particular, low-rank matrices may be approximated as $B \approx U \cdot V^T$, where U and V are narrow rectangular matrices, such that U and V possess fewer entries than B and allow for faster matrix operations. Although the original matrix B will generally not be low-rank, off-diagonal blocks may well be, such that a subdivision of the matrix into blocks is first determined. It may be hierarchical in nature, as used e.g. in the Hierarchically Semi-Separable (HSS) format [16, 17] which further uses binary trees, or flat, as used e.g. in Block-Low-Rank compression (BLR) [18]. The admissibility criterion determining whether a given block should be compressed or not depends on the specific solver at hand.

1.3 Phases in a time step

Now that the JOREK solver, the sparse matrix system, and sparse matrix libraries have been introduced, we identify the major numerical stages performed during a single time step. The stages are abbreviated by one letter in the following to simplify notation in figures and tables later on. Note, that the present article concentrates on the phases after the global matrix construction. Here, **F** and **I** are usually most critical for the overall performance.

- **G: Global matrix construction.** Done in every time step. Can cost a significant fraction of the overall run time depending on the case. Not a topic of the present work, but addressed in Ref. [19] and more thoroughly in future work.

- **P: Extraction of preconditioner matrices.** So far done by extracting from the global matrix via communication; an alternative option for direct construction was implemented for the present work as shown in Section 2.1. This phase also includes time for conversion of preconditioning matrix blocks into CSR format and conversion into complex matrices (where applicable). The last part is typically not negligible, but also not dominating computational costs.

- **A: Analysis of the matrix structure.** Only done in the very first time step of a simulation, since the structure is not changing during a simulation, but only the values of the matrix entries. This phase is therefore usually not critical for the overall performance.

- **F: LU-factorization of the preconditioner matrices.** Done only in time steps where the preconditioner needs to be updated. Often critical for the overall performance. The relative costs compared to phase **I** depend on the application and time step used, but also on the user defined threshold for updating the preconditioning matrix – the user can influence the frequency of the preconditioner updates to some degree via the choice of the time step and via a threshold.

- **I: Iterative solution of the global system** including solver calls for the preconditioner matrix blocks. Done in every time step. Often critical for the overall performance. The relative costs compared to the preconditioner updates of phase **F** depend on case and settings (see explanation above).

1.4 Setup for the numerical tests

The quantities listed in the following are used in this article to describe the benchmark setups and results.

- N_{N}: Total number of compute nodes used in the simulation
- N_{M}: Total number of MPI tasks used in the simulation
- M_{T}: Total memory consumption for the whole simulation (sum for all MPI tasks)
- t_{W}: Elapsed wall clock time
- $t_{\mathrm{N}} \equiv t_{\mathrm{W}} \cdot N_{\mathrm{N}}$: Computational cost in node-hours

All benchmarks performed in this work are carried out on the Marconi supercomputer operated by CINECA. The partition Marconi-Fusion available to the European fusion research community comprises of 2396 compute nodes, each equipped with two 24-core Intel Xeon 8160 CPUs ("Skylake" generation) at a base clock speed of 2.10 GHz and 192 GB DDR4 RAM. The interlink between the compute nodes is provided by Intel OmniPath (100 Gbit/s). We use Intel v.2018.4 compilers with compatible `intelmpi` and `mkl` libraries.

1.5 Outline

The rest of the article is organized as follows. Section 2 describes the developments performed as part of the present work. Subsection 2.1 briefly shows an alternative option for constructing the preconditioning matrices, subsection 2.2 explains new solver interfaces which were implemented as well as the adaptation to complex preconditioning matrices and subsection 2.3 describes a generalization of the preconditioner, which improves convergence in highly non-linear configurations. In Section 3, previously existing and new solver options are compared based on realistic simulation cases to investigate performance improvements obtained in the present work. Finally, Section 4 briefly provides summary, conclusions, and an outlook to future developments.

2 Developments performed in this work

2.1 Construction of preconditioning matrices

The global matrix A_{glob} is constructed in JOREK in a domain decomposed manner, where each MPI task is responsible for a certain fraction of the computational grid (Section 1.1.2). Originally, the individual mode blocks needed for the preconditioner are extracted from the global matrix via expensive MPI all-to-all communication. The drawback of this approach is a strong increase of communication time for a large problem size and an unfavorable scaling with the number of MPI tasks. As part of this work, an option was implemented to calculate the mode blocks directly instead of extracting them from the global matrix to avoid the communication overhead. Here, a group of MPI tasks is responsible for each toroidal mode distributing the work through the domain decomposition. This new approach offers a better parallel scalability than the communication based one (see Section 3.1). The main drawback is that the preconditioner matrix construction needs to be done by direct integration instead of fast Fourier transform (which is used for the global matrix construction), thus some cases exist, where direct construction provides no gain. Further optimization of the direct preconditioner matrix construction is foreseen for the future. Section 3.1 contains a benchmark for this development.

2.2 New solver interfaces

Prior to this work JOREK had interfaces to the sparse matrix solvers MUMPS, PaStiX and WSMP. These libraries are used to solve block-matrix systems in the preconditioner, or optionally to the whole matrix system in case of small problem sizes. In order to reduce memory consumption and execution time we developed complex interface to PaStiX solver and added the new STRUMPACK solver, as described in the following Sections 2.2.1–2.2.2.

The new version 6.x of PaStiX has been released recently providing major revision to the library. Corresponding JOREK interface has been developed [20] allowing usage of new features such as Block-Low-Rank compression.

2.2.1 Complex matrix interface to PaStiX 5.x library

PaStiX can be compiled for real or for complex matrices. An interface has been implemented allowing to use the preconditioner block-matrices in the complex format, which reduces the memory consumption considerably. The transformation into complex format is only possible when the matrix has the appropriate symmetry structure. A structure of the system of equations according to

$$\begin{pmatrix} a & -b \\ b & a \end{pmatrix} \cdot \begin{pmatrix} x \\ y \end{pmatrix} = \begin{pmatrix} c \\ d \end{pmatrix} \tag{1}$$

can be replaced by

$$\big(a + ib\big) \cdot \big(x + iy\big) = \big(c + id\big) \tag{2}$$

Due to some interactions between the $n = 0$ toroidal mode and the $n > 0$ modes that do not obey this symmetry exactly, the following symmetrization is performed:

$$\begin{pmatrix} a & -b \\ c & d \end{pmatrix} \rightarrow \begin{pmatrix} (a+d)/2 & -(b+c)/2 \\ (b+c)/2 & (a+d)/2 \end{pmatrix} \tag{3}$$

This symmetrized matrix can now be replaced by a complex form, analogously to (2). As will be shown later, the approximation introduced by this symmetrization affects the efficiency of the preconditioner only very mildly (small impact on the number of GMRES iterations) such that the overall benefit of using complex matrices prevails. Direct construction in complex format instead of conversion could enhance the performance further, but is left for future work. Besides switching to complex input, nothing else was changed in the PaStiX 5 interface. This implies that also the support for "multiple degrees of freedom", which this solver library offers, is still usable. This feature allows JOREK to specify the size of small dense blocks in the sparse structure, which share the same connectivity and thus can be handled in an identical way in the analysis phase of the solver. A complex matrix interface for STRUMPACK will be implemented soon as well. Tests of the performance of the real matrix interface are presented in Section 3.3.

2.2.2 Interface to the STRUMPACK library

The STRUctured Matrix PACKage – STRUMPACK v.5.0.0 [15] was identified as a promising additional solver library to compare to existing solvers in JOREK. Key features motivating our choice are the capability of handling distributed matrix input, the flexible MPI/OpenMP parallelization including GPU compatibility and the various options (such as BLR and HSS) for compressing the dense frontal matrices. For additional flexibility, as a first step, we developed our own Fortran-C++ interface for STRUMPACK offering routines for initializing, passing the matrix, reordering, factorizing, solving, and finalizing. Sparse matrix is passed to STRUMPACK in row-distributed fashion using the compressed sparse row (CSR) format. The conversion from the coordinate format used in JOREK for the construction into the CSR format has to additionally order the column indices and remove duplicates resulting from the domain decomposition to

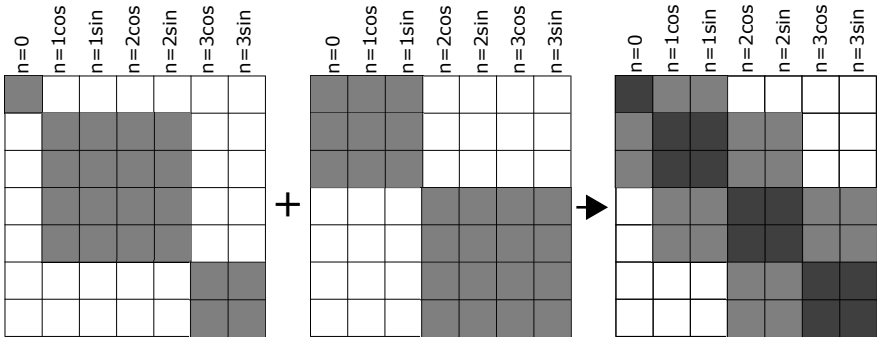

Figure 2: Setup for mode groups denoted as *Overlapping I*. Schematic illustration of linear combination of precondition matrices which combine modes (0,1), (1,2), (2,3), (0), (3) into diagonal blocks. The resulting coverage of elements from the original matrix is shown in the right, with lighter shade representing a factor 1/2 multiplication.

match the expectations by STRUMPACK (while the original matrix ordering is set to match PaStiX requirement). To realize this, the conversion of the sparse matrix format can be performed by a newly implemented interface to the Intel MKL functions or by a newly developed routine performing the same task without library dependencies for best portability. The matrix analysis and fill-reducing reordering is only performed for the first time step in JOREK. In all following time steps, an argument is passed to STRUMPACK which indicates that the structure of the matrix has not changed. For the reordering, METIS is used in this article; optionally also PARMETIS, SCOTCH, or PTSCOTCH can be used. STRUMPACK internally applies an algorithm for achieving large diagonal components and scales entries such that the row scaling performed in JOREK when passing matrices to PaStiX is not needed. A common treatment of small dense blocks ("multiple degrees of freedom"), like available in PaStiX to speed up reordering, is not presently available in STRUMPACK. The performance of the code when using STRUMPACK is assessed in Section 3.2.

2.3 Generalization of the preconditioner for mode groups

In this Section, we describe the most significant development performed within the present work. We explain an approach for improving the efficiency of the preconditioner in highly non-linear scenarios, where the coupling between the toroidal Fourier modes becomes strong causing the GMRES convergence to deteriorate massively or break down entirely. The approach followed here, is to combine several toroidal modes into "mode groups". The interaction between the modes within the mode groups is retained in the preconditioning matrix P. Consequently, larger block-matrices need to be solved than in the original preconditioner, which makes the solution for more expensive in terms of memory consumption and computing time. Nevertheless, capturing the non-linear interaction can improve the convergence of the iterative solver so strongly that

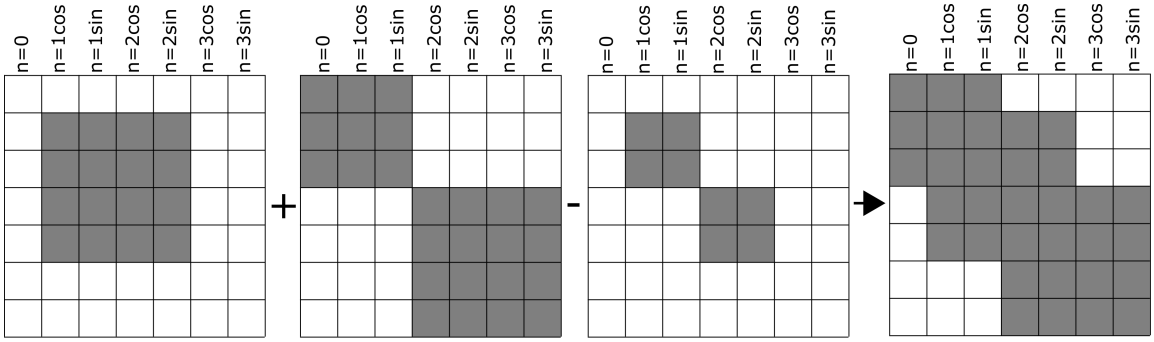

Figure 3: Setup for mode groups denoted as *Overlapping II*. Schematic illustration of linear combination of precondition matrices which combine modes (0,1), (1,2), (2,3), and subtracting (1), (2) modes which have overlapping contributions. Thus, the interaction between neighboring modes is fully accounted for in the preconditioner.

the overall performance is significantly enhanced, as demonstrated in Section 3.4.

Figures 2 and 3 illustrate the approach by two examples. In the first case, referred to as *Overlapping I* (Figure 2), we combine every two neighboring modes into one block and solve each block independently. The preconditioner solution is constructed by placing solutions of individual blocks in corresponding rows of a full solution vector. Solutions from the overlapping blocks are summed up with a factor 1/2. When comparing to the standard approach, where we solve N single-mode blocks, the new method requires solution of $N + 1$ blocks of larger size, where N is the total number of toroidal modes; $N = 4$ in the present example. In the described approach we effectively take into account interactions of neighboring modes which physically resemble to mode coupling as observed in turbulence cascading.

Since in the *Overlapping I* method, neighboring mode coupling is effectively taken into account with a factor of 1/2, we consider an alternative method referred to as *Overlapping II* (Figures 3). Here we also combine the neighboring modes into blocks, but instead of multiplying corresponding contributions to the full preconditioner solution by 1/2, we subtract the solutions for individual modes (except the first and the last one, which don't overlap). Thus, here we have to solve $2N-3$ blocks in total: $N-1$ combined blocks and $N - 2$ individual mode blocks.

The implementation is performed in a very general way allowing more advanced configurations for mode groups than the two examples given. It is, for instance, possible to combine modes separated by a certain toroidal period, modes which are believed to have the strongest interactions, or the interaction of each $n \neq 0$ mode with $n = 0$. The implementation in JOREK is done as follows:

- Via the namelist input file, arbitrary mode groups can be constructed in a flexible way. Each mode group forms a diagonal block in the preconditioner matrix.

- The number of MPI tasks for each mode group can be automatically assigned

according to the number of non-zero entries in each mode group, or manually be chosen via the input file. This allows optimizing load balance for non-uniform matrix block sizes.

- Mode groups can be overlapping. When reconstructing the whole matrix system $P\,y = c$ solution as linear combination of the individual solutions from the mode group blocks, factors are applied. For example, the factor is $1/2$ in the *Overlapping I* case and factor ± 1 in case of the *Overlapping II* example.

Mode group methods are benchmarked in Section 3.4 with the standard preconditioner.

3 Benchmarks for the developments performed

Now that we have introduced the developments performed to improve the numerical efficiency of the JOREK solver and preconditioner in the previous section, a set of real-life simulation cases is taken as basis to evaluate the performance of the methods. Each case is briefly explained in the respective subsection. To save computational time, not all solver options are tested for all cases. Note that most developments are already used in production by the JOREK community at the time of submission of this article.

3.1 Preconditioner matrix assembly

Here, we compare the performance and parallel scalability of the preconditioner matrix assembly via communication and by direct construction. The benchmark is based on a simplified simulation of edge localized modes (ELM) in a JET-like geometry, i.e., an X-point plasma with open and closed field lines included in the simulation domain. A fairly high poloidal grid resolution of 51k Bezier finite elements is used, while only the toroidal mode numbers $n = (0, 4, 8)$ are included in the simulation. Tests for this case are performed both in the linear phase, where the exponentially growing instabilities are too small to modify the axisymmetric $n = 0$ component and in the non-linear phase during the collapse of the edge pressure gradient caused by the instability.

The simulations are performed on 6 to 96 compute nodes (N_N) with 2 MPI tasks per node and 24 OpenMP threads per MPI task. Simulation timing results are shown in Table 1. With 6 compute nodes, the direct construction is two times more efficient than the communication and scales well with a further increasing the number of compute nodes. The communication exhibits poor scaling with the numbers of MPI tasks, as expected. Nevertheless, it is worth mentioning that in realistic simulations, one does not use such a large number of compute nodes due to limited scalability of the solver hence the performance of direct construction should be further optimized in the future.

3.2 Comparison of PaStiX and STRUMPACK solver performance

To measure parallel scalability and relative performance of PaStiX 5.x and STRUMPACK solvers we consider the same case as in the previous section. Two different resolutions

N_{N}	communication	direct construction
6	46.07	21.34
12	40.55	10.96
24	38.25	5.64
48	39.48	3.12
96	35.94	1.76

Table 1: Measurements for preconditioning matrix assembly (phase **P**). The wall-clock time t_{W} (sec) spent in assembling distributed preconditioner block-matrices using communication and direct construction is compared as function of the number of compute nodes N_{N}.

with 13745 poloidal grid nodes (LR=low resolution) and 51470 grid nodes (HR=high resolution) are considered here. First, we compare the performance of both PaStiX and STRUMPACK libraries for the LR case with $n = (0, 4, 8)$ to avoid too strict memory per node constraints which would limit the flexibility in the number of MPI tasks per node (in particular for PaStiX). We consider 6 compute nodes and scan the number of MPI tasks per node, while adjusting the number of OpenMP threads, accordingly. The results are shown in Figures 4–6. As we can see, the STRUMPACK solver shows considerably better efficiency at a larger number of MPI tasks per node, while the PaStiX performance is less sensitive to this parameter. For the LU factorization, PaStiX shows unfavorable scaling with more than four MPI tasks per node. Besides solver performance, an important factor for choosing the optimal parameter regime is the time spent on constructing the global sparse matrix. As can be seen from Figure 7, it is most efficient at 4-8 tasks per node for this case. We observe the same trend for the full-size simulation as well. Thus, the decision for selecting MPI tasks per node depends on the ratio of time spent on constructing global matrices to the time spent on GMRES iterations. Finally, due to the ability to provide the distributed matrix directly to the solver and due to better memory efficiency, the maximum memory utilization can be significantly lower with the STRUMPACK library as shown in Figure 8. The difference in memory consumption partially results from the fact that the PaStiX 5.x requires each responsible MPI task to have a copy of the full preconditioner block-matrix, while the matrix is row-wise distributed across MPI tasks in case of the STRUMPACK. The higher memory consumption when running with the PaStiX library may limit the ability to choose the optimal number of MPI tasks per node.

For the HR case, the production-size ELM case with $n = (0, 4, 8)$, the number of entries in the sparse matrix (number of nonzero entries $nnz = 1.4 \times 10^9$) requires using at least six compute nodes with at least two MPI tasks per node to avoid integer overflow when constructing the global matrix. For optimal performance, it is beneficial to increase the number of MPI tasks per node, however, due to higher memory consumption of the PaStiX solver (Figure 9, left panel) we are limited to two MPI tasks per node with PaStiX. With STRUMPACK, we can use up to eight MPI tasks per node. The

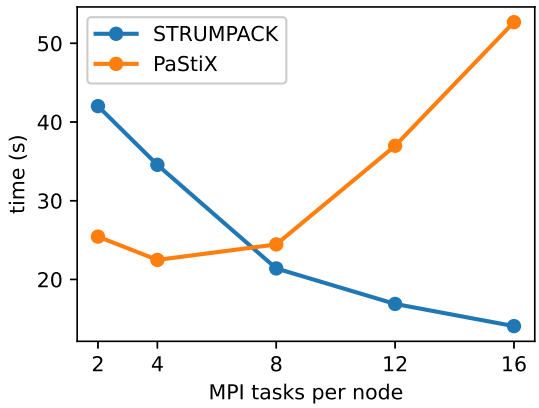

Figure 4: Time spent on LU factorization (**F**) in the the LR simulation case using 6 compute nodes

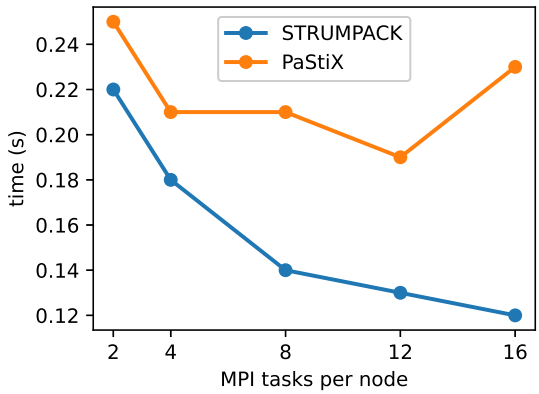

Figure 5: Time spent on solve (part of phase **I**) in the LR simulation case using 6 compute nodes

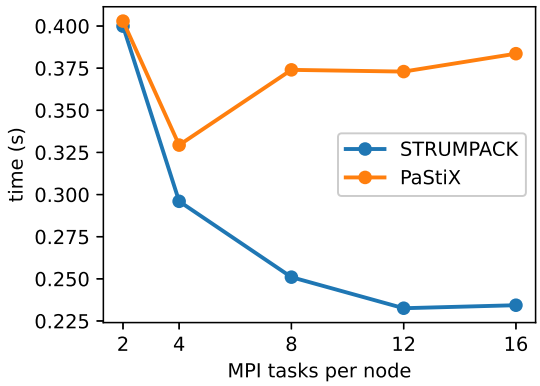

Figure 6: Time spent on each consecutive GMRES iteration (part of phase **I**) in the LR simulation case using 6 compute nodes

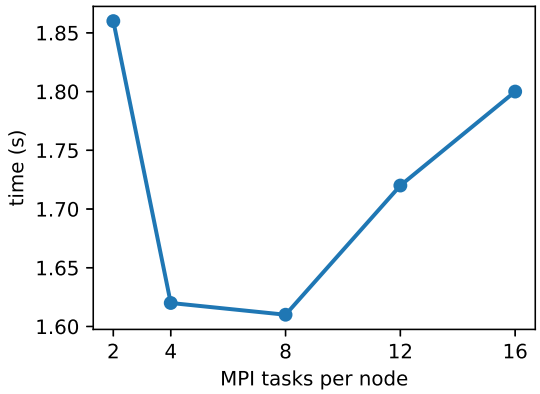

Figure 7: Time spent on constructing the global sparse matrix (**G**) in the LR simulation case using 6 compute nodes

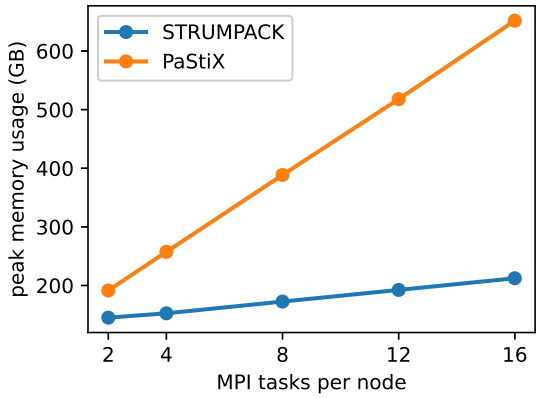

Figure 8: Peak memory consumption M_T in the LR simulation case using 6 compute nodes

corresponding memory consumption when using the STRUMPACK solver is shown in Figure 9, right panel.

		PaStiX	STRUMPACK
A	Analysis	20.5	87.9
F	Factorization	136.4	148.7
I	Solve	0.74	0.53
	First GMRES iteration	4.65	3.41
	Consecutive GMRES iteration	1.36	1.08

Table 2: Wall-clock time t_{W} (sec) spent on different solver phases in the HR simulation using $N_{\mathrm{N}} = 6$ compute nodes with $N_{\mathrm{M}}/N_{\mathrm{N}} = 2$ MPI tasks per node (PaStiX) and $N_{\mathrm{M}}/N_{\mathrm{N}} = 8$ MPI tasks per node (STRUMPACK).

In Table 2, we show the elapsed wall clock times for the comparison between the PaStiX and STRUMPACK solvers for the HR case. For simulations in X-point geometry, STRUMPACK needs to do a permute and scale procedure to put large entries on the diagonal. This can increase the analysis time (**A**) significantly. On the other hand, for PaStiX, a column scaling needs to be performed in JOREK, for which the corresponding time is not included here, as it is part of the preconditioner matrix assembly (**P**). In the case considered here, PaStiX performs 9% faster on the numerical factorization task (**F**). Meanwhile, STRUMPACK shows better performance in the solve phase (**I**) with an improvement by 36% in the first GMRES iteration and 26% improvement in each consecutive iteration (note that the actual solve is shown separately in the table for reference, but is part of the GMRES iterations). Taking this into account, in a simulation with 20 GMRES iterations per time step, the overall performance of both solvers becomes comparable when the preconditioner update (i.e., a re-factorization) takes place every four time steps. For more frequent updates the PaStiX solver is preferable. If preconditioner updates are required less frequently, the STRUMPACK provides better performance.

To address the performance scaling with the number of processors (strong scaling), we have simulated the LR case with $n = (0, 4, 8)$ toroidal modes using 3, 6 and 12 compute nodes with 8 MPI tasks per node using the STRUMPACK library. The results are presented in Table 3. It is shown that the sparse matrix construction and solve tasks scale relatively well with a factor of about 1.5 time reduction per doubling of number of nodes. A considerable fraction of the GMRES iteration time is spent on MPI communication, which impairs the strong scaling. The remaining matrix-vector multiplication part of GMRES iteration can potentially be further improved. Note, that production simulations with JOREK are usually performed at the lowest number of compute nodes permitted from the memory consumption, such that the weak scaling discussed in the next paragraph is of a higher practical relevance.

We have investigated the weak scaling performance of JOREK based on the LR simulation using STRUMPACK. In addition to $n = (0, 4, 8)$, we have considered cases with

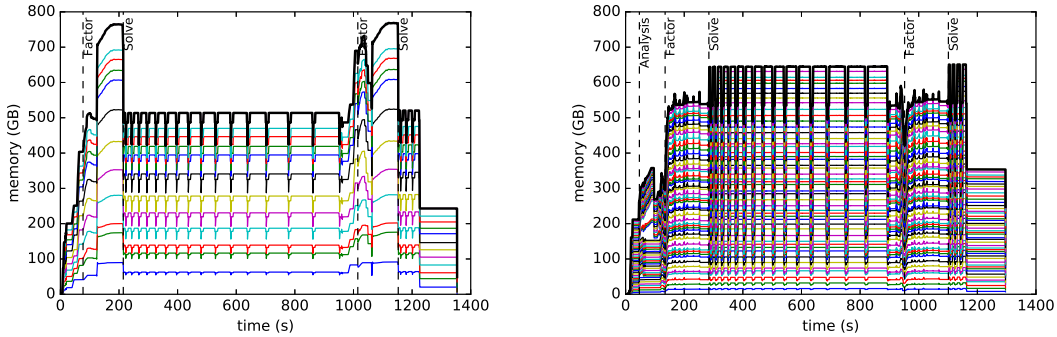

Figure 9: Cumulative plot of memory utilization per individual MPI task in the HR simulation case with PaStiX using $N_{\mathrm{N}} = 6$, $N_{\mathrm{M}} = 12$ (left panel) and STRUMPACK, using $N_{\mathrm{N}} = 6$, $N_{\mathrm{M}} = 48$ (right panel).

	Compute nodes	3	6	12
G	Global Matrix Construction	2.74	1.57	1.04
I	Solve	0.21	0.14	0.10
	First GMRES iteration	1.28	1.0	0.84
	Consecutive GMRES iteration	0.34	0.25	0.20

Table 3: Wall-clock time t_{W} (sec) spent on solver tasks for different number of compute nodes using STRUMPACK while keeping the problem size fixed (strong scaling).

higher toroidal mode numbers $n = (0, 2, 4, 6, 8)$ and $n = (0, 1, 2, \ldots, 8)$ here. For this simulations we have used 6, 10 and 18 compute nodes, respectively (i.e. 2 nodes per one toroidal mode), with 8 MPI tasks per node. Since the preconditioner matrix block sizes remain the same for all three cases, the time spent on analysis, LU factorization, and solve tasks remains the same, while the GMRES communication time increases with the number of toroidal modes. The corresponding simulation results are shown in Table 4. With a higher number of toroidal modes, the time spent on constructing the global matrix remains roughly constant, since the number of matrix entries per MPI task doesn't change significantly. Meanwhile, the time spent on GMRES iterations increases linearly due to increased communication time. The overall performance scaling depends on the relative contributions of matrix construction time and GMRES iteration time.

3.3 Comparison between real and complex solvers in the preconditioner

To compare the performance of real and complex PaStiX solvers, we have considered the same case as in Section 3.1. Table 5 contains data from the simulations restarted in the highly nonlinear regime for a single time-step on 6 and 3 compute nodes with 2 MPI tasks per node. For the given problem size, the real (PaStiX) solver needs at

	Toroidal modes	$0, 4, 8$	$0, 2, \ldots, 8$	$0, 1, \ldots, 8$
G	Global Matrix Construction	1.57	1.13	1.13
I	First GMRES iteration	1.0	1.46	2.61
	Consecutive GMRES iteration	0.25	0.37	0.61

Table 4: Wall-clock time t_{W} (sec) spent on solver tasks for different number of toroidal modes using STRUMPACK while increasing the toroidal resolution accordingly (weak scaling).

least 6 compute nodes based on the memory requirement. The complex (PaStiX) solver, on the other hand, can be executed on 3 compute nodes due to the reduced memory consumption.

PaStiX solver		real	complex	
number of compute Nodes		6	6	3
A	Analysis	22.71	14.98	11.50
F	Factorization	133.38	53.40	81.27
I	Solve	1.22	0.83	1.46
	Number of GMRES iterations	25	26	26
	GMRES solve	42.49	34.31	47.24

Table 5: Wall-clock time t_{W} (sec) spent on solver phases using 6 compute nodes for the real PaStiX solver and 6 resp. 3 compute nodes for the complex PaStiX solver.

In Table 5, we compare the wall-clock time t_{W} (sec) spent on solver phases using 6 compute nodes for real (PaStiX solver) and 6 respectively 3 compute nodes for complex (PaStiX solver). Due to the reduced matrix dimension, factorization (**F**) as one of the most expensive parts of the solve step is roughly 2.5 and 3.3 times faster when using the complex solver on 6 and 3 compute nodes, respectively, compared to the real solver. The analysis (**A**) is also done more efficiently with the complex solver, however, being performed only in the first time step, it adds limited benefits for a typical simulation. Moreover, one can notice from the Table 5 that although the complex solver requires one additional GMRES iteration as compared to the real solver, the GMRES solve (**I**) on 6 respectively 3 compute nodes is more efficient by a factor of 1.2 and 1.8 as compared to the real solver on 6 compute nodes.

Figure 10 shows the time-lines of the memory consumption for the real solver (with 6 compute nodes) and complex solver (with 6, 3 compute nodes). It is apparent that the maximum memory consumption when using the complex solver with 6 nodes is roughly 600 GB, which is less than roughly 700 GB in the case of the real solver. The memory consumption is even lower in the case on complex solver using 3 compute nodes. Thus, we

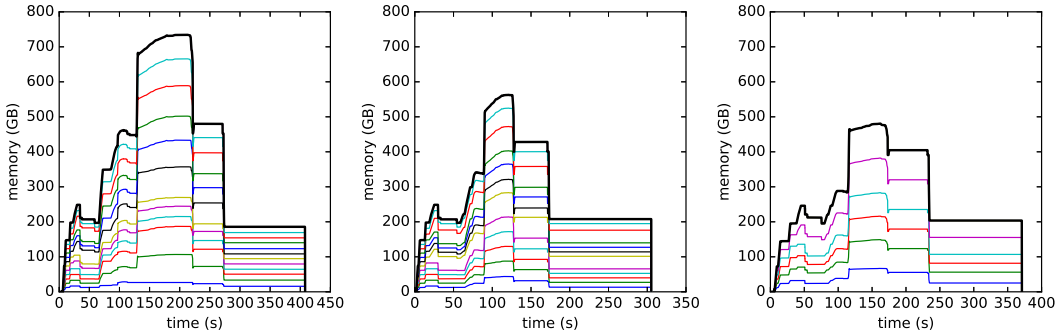

Figure 10: Cumulative plot of memory utilization per individual MPI task in the HR simulation case with real (left panel) and complex (middle panel) PaStiX solver using 6 compute nodes, and complex PaStiX solver using 3 compute nodes (right panel)

confirm that the complex solver reduces the overall memory consumption significantly. It is worth mentioning that we observe a larger reduction in memory consumption for a higher number of toroidal modes.

In conclusion, it can be seen from Table 5, that the overall performance gain by the complex solver is moderate when the memory consumption imposes the same minimum number of compute nodes for the real and complex solvers and when updates of the preconditioning matrix (factorizations) are needed seldomly. On the other hand, if the preconditioning matrix is updated more often, the complex solver may reduce the total computational cost (including matrix construction and preconditioner matrix assembly which are not explicitly discussed in this section) by a third. When the reduced memory consumption by the complex solver allows to use a lower number of compute nodes, the overall computational costs can be approximately halved due to the limited scalability of the solver.

3.4 Assessment of computational efficiency with mode groups in the preconditioner

The simulation considered here is a slightly adapted version of the simulations presented in Ref. [21]. It represents a vertically unstable plasma (vertical displacement event, VDE), that develops violent non-axisymmetric ($n \neq 0$) instabilities while moving into the plasma facing components. We have chosen this case, since the standard iterative solver convergence is poor, forcing the use of extremely small time steps. It is suspected that the strong non-linearity of the problem reduces the accuracy by which the preconditioning matrix P approximates the complete system A, such that condition number and convergence deteriorate.

We have used this VDE case to test the new preconditioner based on the overlapping mode groups. For this purpose we run simulations in the nonlinear regime, and compare the "standard" preconditioner (Fig. 1 right) with two new approaches based on

overlapping mode groups (Figs. 2 and 3).

		Standard	Overlapping I	Overlapping II
A	Analysis time (s)	27.0	99.5	99.2
F	Factorization time (s)	21.1	123.9	123.8
I	Solve time (s)	0.12	0.34	0.34
	GMRES iteration time (s)	47.3	21.3	16.7
	Number of GMRES iterations	130	43	32

Table 6: Comparison of solver performance of $n = (0, 1, 2, 3)$ VDE case with $\Delta t = 0.05$, based on 10 time steps run with the STRUMPACK solver using 8 compute nodes.

		Standard	Overlapping I
A	Analysis time (s)	24.6	126.5
F	Factorization time (s)	22.2	147.4
I	Solve time (s)	0.13	0.40
	GMRES iteration time (s)	87.8	42.8
	Number of GMRES iterations	97	45

Table 7: Comparison of solver performance of $n = (0, 1, 2, \ldots, 10)$ VDE case with $\Delta t = 0.05$, based on 10 time steps run with STRUMPACK solver using 22 compute nodes.

As shown in Table 6, the *Overlapping I* and *Overlapping II* preconditioners reduce the number of GMRES iterations by a factor of 3 and 4, respectively, leading to the reduction of the whole GMRES cycle time by a factor of 2.2 and 2.8, respectively. Meanwhile, the factorization time increased by a factor of 6. Thus, the overall performance strongly depends on how often preconditioner updates are required. A similar improvement trend with *Overlapping I* method is observed for the $n = (0, 1, 2, \ldots, 10)$ VDE case as shown in Table 7. Here we do not use the *Overlapping II* preconditioner due to its higher computational cost.

The analysis, factorization and solve times with the new preconditioner are determined by the corresponding times spent on the largest diagonal block, which is twice the size of the standard case. Since each diagonal block-matrix is factorized and solved independently, the difference in matrix sizes introduces a strong workload imbalance. To address this, we have implemented a flexible distribution of MPI tasks to each mode group. For example, in the current simulation using the *Overlapping I* method, we have five mode groups and a total of 32 MPI tasks. The groups consist of the following toroidal modes: (0),(0,1),(1,2),(2,3),(3). The block size corresponding to $n = 0$ mode is twice smaller than for any other mode, and the number of nonzero entries is 4 times smaller. The

preconditioner block-matrix sizes for each group are shown in Table 8.

Mode sets	(0)	(0,1)	(1,2)	(2,3)	(3)
Matrix rank	200,767	602,301	803,068	803,068	401,534
nnz	52,808,329	475,274,961	844,933,264	844,933,264	211,233,316

Table 8: Ranks and numbers of nonzero entries in preconditioner matrices for $n = (0, 1, 2, 3)$ VDE case using the Overlapping I preconditioning method.

There are different ways to distribute the available 32 MPI tasks among the mode groups. For instance, distributing them as (2,6,9,9,6) would increase the factorization time to 147.6 sec as compared to 123.9 sec in the case of (1,4,12,12,3) tasks per group distribution. Here one should take into account that the most computationally expensive factorization has different MPI task scaling compared to the GMRES iteration cycle, thus the task distribution for balanced performance would depend on the relative contribution of total factorization time and total iteration time. However, as a rule of thumb, one can distribute tasks roughly proportionally to the number of nonzero entries in each mode group. In $n = (0, 1, 2, 3)$ we have assigned 1 and 3 MPI tasks to the single mode groups of the (0) and the (3) modes, respectively, 4 tasks to the $(0, 1)$ group, and 12 tasks to each of the $(1, 2)$ and the $(2, 3)$ groups. In the $n = (0, 1, 2, \ldots, 10)$ case 2 MPI tasks are assigned to the smallest mode group of (0) mode, 6 MPI tasks are assigned to the mode group of (11) mode, and the overlapping mode groups get 8 MPI tasks each.

Since the preconditioning matrix needs not to be updated (factorized) in every time step, the efficiency of the new preconditioner is determined by the actual frequency of these updates. In our example, the *Overlapping I* preconditioner would lead to the same overall performance, if the preconditioner is updated every five time steps. This number would be slightly higher in practice, since the time to construct preconditioner matrices is also slightly higher for the new preconditioner. In the nonlinear phase of the VDE simulation with a normalized time step of 0.05, the preconditioner matrix updates need to be performed approximately every 50 time steps, which gives the new preconditioners a strong advantage.

Meanwhile, as the preconditioner approximates the total system a lot better now, it becomes possible to increase the simulation time step allowing for an even more efficient way of running the simulation. For the same nonlinear case, good overall performance was obtained when increasing the time step by a factor of 3, both for the *Overlapping I* and *Overlapping II* preconditioners, leading to the total t_{W} spent on simulating 100 steps using 8 compute nodes being equal 104 min and 95 min, respectively. Comparing this to 97 min required to perform 100 steps with $\Delta t = 0.05$ using the standard preconditioner, an approximate speed-up of a factor $3\times$ is obtained. The same conclusion holds for the VDE case with a higher toroidal resolution including the $n = (0, \ldots, 10)$ toroidal modes, which was tested as well.

The main disadvantage of the new preconditioner lies in the increased memory consumption. As we can see in the Figure 11, for the VDE case with $n = (0, 1, 2, 3)$, the

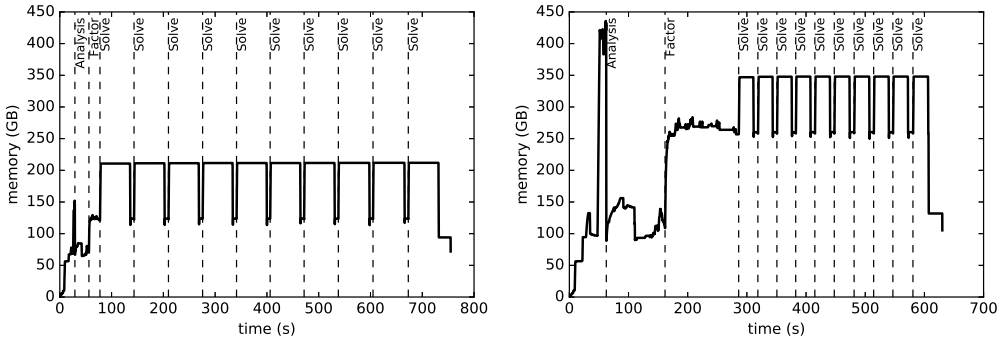

Figure 11: Cumulative memory consumption in $n = (0, 1, 2, 3)$ VDE case simulation with standard preconditioner (left panel) and Overlapping I preconditioner (right panel) using 8 compute nodes with 4 MPI tasks per node

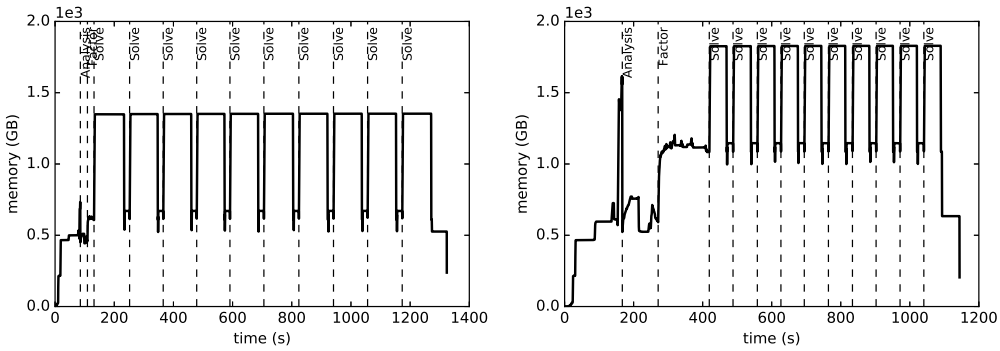

Figure 12: Cumulative memory consumption in $n = (0, 1, \ldots, 10)$ VDE case simulation with standard preconditioner (left panel) and Overlapping I preconditioner (right panel) using 22 compute nodes with 4 MPI tasks per node

maximum required memory with the new preconditioner was twice as large as the standard one. With the direct construction of the preconditioning matrix, the initial peak around $t = 50$s would disappear such that the maximum memory utilization is in the "solve" phase and the difference between both methods is reduced to about 50%, like we observe in the Figure 12 for the $n = (0, 1, 2, \ldots, 10)$ case. Combining mode groups and complex solver will be investigated in the future as a measure for reducing memory consumption.

The presented results demonstrate just an example of using the new preconditioner. With the provided implementation flexibility, there is room for further performance improvements, e.g. by adjusting work load balance, data locality, optimization of GMRES preconditioner update frequency vs. simulation time step, etc.

4 Summary

In this article, we have described the iterative solver with the physics-based preconditioner (PC) used in the non-linear MHD code JOREK, the properties of the sparse matrix system, and the interfaces to parallel sparse matrix solver libraries. We also explained some limitations faced with this solver in particular regarding memory consumption and convergence in highly non-linear scenarios.

For the PaStiX 5.x library the new interface was developed, which allows using complex numbers in the preconditioner, leading to the improved performance and memory utilization. Reduced memory consumption with complex preconditioner allows to operate a code with less nodes and thus allows to shift the point of operation towards the lower (ideal) part of the strong scaling curve.

The STRUMPACK library has been added to JOREK as a new solver option, providing several performance benefits, such as ability to use distributed matrices, more efficient memory utilization, and overall solver speed-up.

The new direct method for constructing preconditioner matrices in a distributed fashion is implemented, which avoids expensive all-to-all MPI communication. This results in potentially significant improvement of performance, depending on the case considered.

Finally, the most important development, is a generalization of the preconditioner to the "mode groups". The new method allows capturing some of the non-linear mode coupling in the PC by combining several toroidal modes in the diagonal matrix blocks, which can be solved independently. Such preconditioner much better resembles the original system, thus leading to major improvement of the GMRES convergence and, consequently, to significant reduction of the overall run time in the non-linear simulation regime. Besides the benefits for tokamak simulations, the mode groups will also be an essential building block to make future JOREK simulations of stellarator cases [22, 23] possible, where instabilities do not linearly decouple in the toroidal modes any more.

Acknowledgements

The authors would like to thank Omar Maj for fruitful discussions, and FJ Artola, A Cathey, F Wieschollek, I Krebs, R Ramasamy for providing "real-life" test cases, Mathieu Faverge and the rest of the PaStiX team for their assistance with PaStiX 6. One of the author (I.H.) would like to thank Sebastian Ohlmann (MPCDF) and Pieter Ghysels (LBNL) for technical advising.

Part of this work has been carried out within the framework of the EUROfusion Consortium and has received funding from the Euratom research and training program 2014-2018 and 2019-2020 under grant agreement No 633053. The views and opinions expressed herein do not necessarily reflect those of the European Commission. Some of the work was performed using the Marconi-Fusion supercomputer.

References

[1] G.T.A. Huysmans and O. Czarny. MHD stability in X-point geometry: simulation of ELMs. *Nuclear Fusion*, 47(7):659, 2007. doi:10.1088/0029-5515/47/7/016.

[2] M Hoelzl, G T A Huijsmans, S J P Pamela, M Becoulet, E Nardon, F J Artola, B Nkonga, C V Atanasiu, V Bandaru, A Bhole, D Bonfiglio, A Cathey, O Czarny, A Dvornova, T Feher, A Fil, E Franck, S Futatani, M Gruca, H Guillard, J W Haverkort, I Holod, D Hu, S K Kim, S Korving, I Krebs, G Latu, F Liu, P Merkel, D Meshcheriakov, S Mochalskyy, J A Morales, R Nies, N Nikulsin, F Orain, J Pratt, R Ramasamy, P Ramet, C Reux, N Schwarz, P Singh Verma, S Smith, C Sommariva, E Strumberger, D van Vugt, M Verbeek, E Westerhof, F Wieschollek, J Zielinski, and the JOREK Team. The jorek non-linear extended mhd code and applications to large-scale instabilities and their control in magnetically confined fusion plasmas. *Nuclear Fusion*, submitted, 2020. preprint at https://arxiv.org/abs/2011.09120.

[3] F. Orain, M. Bécoulet, G. Dif-Pradalier, G. Huijsmans, S. Pamela, E. Nardon, C. Passeron, G. Latu, V. Grandgirard, A. Fil, A. Ratnani, I. Chapman, A. Kirk, A. Thornton, M. Hoelzl, and P. Cahyna. Non-linear magnetohydrodynamic modeling of plasma response to resonant magnetic perturbations. *Physics of Plasmas*, 20(10):102510, 2013. doi:10.1063/1.4824820.

[4] S. J. P. Pamela, A. Bhole, G. T. A. Huijsmans, B. Nkonga, M. Hoelzl, I. Krebs, and E. Strumberger. Extended full-MHD simulation of non-linear instabilities in tokamak plasmas. *Physics of Plasmas*, 27(10):102510, 2020. doi:10.1063/5.0018208.

[5] Olivier Czarny and Guido Huysmans. Bezier surfaces and finite elements for MHD simulations. *Journal of Computational Physics*, 227(16):7423 – 7445, 2008. ISSN 0021-9991. doi:10.1016/j.jcp.2008.04.001.

[6] M Hoelzl, P Merkel, G T A Huysmans, E Nardon, E Strumberger, R McAdams, I Chapman, S Günter, and K Lackner. Coupling JOREK and STARWALL codes for non-linear resistive-wall simulations. *Journal of Physics: Conference Series*, 401:012010, dec 2012. doi:10.1088/1742-6596/401/1/012010.

[7] Daniël Cornelis van Vugt. *Nonlinear coupled MHD-kinetic particle simulations of heavy impurities in tokamak plasmas*. PhD thesis, Technische Universiteit Eindhoven, Department of Applied Physics, 7 2019. URL https://research.tue.nl/en/publications/nonlinear-coupled-mhd-kinetic-particle-simulations-of-heavy-imp Proefschrift.

[8] Théo Mary. *Block Low-Rank multifrontal solvers: complexity, performance, and scalability*. PhD thesis, University of Toulouse, France, 11 2017. URL http://mumps.enseeiht.fr/doc/Thesis_TheoMary.pdf.

[9] George Karypis and Vipin Kumar. A fast and high quality multilevel scheme for partitioning irregular graphs. *SIAM Journal on scientific Computing*, 20(1):359–392, 1998. doi:10.1137/S1064827595287997.

[10] François Pellegrini and Jean Roman. Scotch: A software package for static mapping by dual recursive bipartitioning of process and architecture graphs. In Heather Liddell, Adrian Colbrook, Bob Hertzberger, and Peter Sloot, editors, *High-Performance Computing and Networking*, pages 493–498, Berlin, Heidelberg, 1996. Springer Berlin Heidelberg. ISBN 978-3-540-49955-8.

[11] Pascal Hénon, Pierre Ramet, and Jean Roman. PaStiX: A High-Performance Parallel Direct Solver for Sparse Symmetric Definite Systems. *Parallel Computing*, 28(2):301–321, 2002. URL https://hal.inria.fr/inria-00346017.

[12] Grégoire Pichon, Eric Darve, Mathieu Faverge, Pierre Ramet, and Jean Roman. Sparse supernodal solver using block low-rank compression: Design, performance and analysis. *Journal of Computational Science*, 27:255 – 270, 2018. ISSN 1877-7503. doi:10.1016/j.jocs.2018.06.007.

[13] P. R. Amestoy, I. S. Duff, J. Koster, and J.-Y. L'Excellent. A fully asynchronous multifrontal solver using distributed dynamic scheduling. *SIAM Journal on Matrix Analysis and Applications*, 23(1): 15–41, 2001. doi:10.1137/S0895479899358194.

[14] Patrick R. Amestoy, Abdou Guermouche, Jean-Yves L'Excellent, and Stéphane Pralet. Hybrid scheduling for the parallel solution of linear systems. *Parallel Computing*, 32(2):136 – 156, 2006. ISSN 0167-8191. doi:10.1016/j.parco.2005.07.004. Parallel Matrix Algorithms and Applications (PMAA'04).

[15] P. Ghysels, S. L. Xiaoye, C. Gorman, and F. Rouet. A robust parallel preconditioner for indefinite systems using hierarchical matrices and randomized sampling. In *2017 IEEE International Parallel and Distributed Processing Symposium (IPDPS)*, pages 897–906, May 2017. doi:10.1109/IPDPS.2017.21.

[16] S. Chandrasekaran, M. Gu, and T. Pals. A fast ulv decomposition solver for hierarchically semiseparable representations. *SIAM Journal on Matrix Analysis and Applications*, 28(3):603–622, 2006. doi:10.1137/S0895479803436652.

[17] Jianlin Xia, Shivkumar Chandrasekaran, Ming Gu, and Xiaoye S. Li. Fast algorithms for hierarchically semiseparable matrices. *Numerical Linear Algebra with Applications*, 17(6):953–976, 2010. doi:10.1002/nla.691.

[18] Patrick Amestoy, Cleve Ashcraft, Olivier Boiteau, Alfredo Buttari, Jean-Yves L'Excellent, and Clément Weisbecker. Improving multifrontal methods by means of block low-rank representations. *SIAM Journal on Scientific Computing*, 37(3):A1451–A1474, 2015. doi:10.1137/120903476.

[19] Tamas B. Fehér, Matthias Hoelzl, Guillaume Latu, and G. T. A. Huijsmans. Performance analysis and optimization of the JOREK code for many-core CPUs. *arXiv e-prints*, abs/1810.04413, 2018. URL `http://arxiv.org/abs/1810.04413`.

[20] R Nies and M Hoelzl. Testing performance with and without block low rank compression in MUMPS and the new PaStiX 6.0 for JOREK nonlinear MHD simulations. *arXiv e-prints*, page arXiv:1907.13442, Aug 2019. URL `https://arxiv.org/abs/1907.13442`.

[21] F. J. Artola, C.R. Sovinec, Jardin S.C., M. Hoelzl, I. Krebs, and C. Clauser. 3D simulations of vertical displacement events in tokamaks: A benchmark of M3D-C1, NIMROD and JOREK. *Physics of Plasmas*, submitted, 2020. preprint at `https://arxiv.org/abs/2011.04523`.

[22] N Nikulsin, M Hoelzl, A Zocco, S Guenter, and K Lackner. A three-dimensional reduced MHD model consistent with full MHD. *Physics of Plasmas*, 26:102109, 2019. doi:10.1063/1.5122013. preprint at `http://arxiv.org/abs/1907.12486`.

[23] Rohan Ramasamy, Matthias Hoelzl, and et al. Extending the JOREK code to 3D simulation grids. private communication, 2020-12-12.